Bloch wave theory of modulational polarization instabilities in birefringent optical fibers

Stefano Trillo
Fondazione Ugo Bordoni, Via Baldassarre Castiglione 59, 00142 Roma, Italy

Stefan Wabnitz
Laboratoire de Physique, Universite de Bourgogne, Faculté de Sciences Mirande, Avenue A. Savary, Boîte Postale n. 400, 21011 Dijon, France

(Received 10 December 1996)

The modulational instability gain spectra, of an arbitrarily polarized intense pump wave that experiences periodic nonlinear polarization rotation in a birefringent optical fiber, are derived by Floquet analysis. The predictions of the linearized analysis are confirmed by numerical simulations of the coupled nonlinear Schrödinger equations. [S1063-651X(97)01907-7]

PACS number(s): 42.81.Gs, 42.65.Sf, 42.65.Ky

I. INTRODUCTION

Over the last ten years, there has been growing research activity in nonlinear mode coupling phenomena in optical fibers and waveguides. The interest in this work was motivated by the applicative demand of ultrafast all-optical signal processing devices that may operate in the frequency range of tens of GHz and higher, that is beyond the capabilities of electronics. A typical successful example of an application of nonlinear mode coupling effects is given by the nonlinear polarization response of optical fibers, which permits ultrashort pulse generation through pulse reshaping and equivalent fast saturable absorber action in fiber-based lasers. Moreover, nonlinear polarization effects also play an important role in all-optical processing devices, such as, nonlinear optical loop mirrors and in fiber-based transmission systems. Another basic example of a nonlinear device for which the same type of coupled-mode description holds, is given by the nonlinear directional coupler, first proposed by Jensen [1].

In this work, we intend to analyze the role of nonlinear polarization rotation of the pump [2–5] on parametric amplification or modulational instability (MI) effects in birefringent nonlinear media, taking an optical fiber as the most relevant example. In fact, as we shall see, in the presence of spatial instabilities for the continuous wave (cw) evolution of the pump [5–8], the large nonlinear polarization changes that occur when the pump wave is close to (but not exactly on) an unstable eigenmode of polarization may lead to substantial variations to the parametric gain spectra of a frequency detuned signal. Although MI of intense polarized beams in birefringent fibers is an issue of relevance for several of the above listed applications, earlier analyses of parametric gain were restricted to the simplest cases where no pump polarization rotation occurs. In fact, the known cases involve a pump beam that is either coupled to a principal birefringence axis [9–13], or equally split between these axes in a highly birefringent fiber [14–18]. We show here that Bloch or Floquet theorem permits the linear stability analysis of a pump wave with an arbitrary input polarization state. In fact, the full pump-power dependence of the modulational instability (MI) gain spectra is derived here. We confirm the results of the linear stability analysis by means of the direct simulation of the coupled nonlinear Schrödinger equations for the two polarization components of the field in the fiber [9]. We believe that the present analysis is important for describing the experimental results [13,19,20] and for assessing the possibility of exploiting MI gain in all-optical processing devices. Moreover, the present approach could be easily extended to assess the role of parametric amplification in several different mode-coupling phenomena.

II. EVOLUTION EQUATIONS

The coupled equations for the two circular polarization components of the pump wave read [9,16]

$$i\frac{\partial A_+}{\partial Z}+i\frac{v}{2}\frac{\partial A_-}{\partial T}-\frac{k''}{2}\frac{\partial^2 A_+}{\partial T^2}+\beta A_+ +\frac{\Delta\beta}{2}A_- + \frac{2R}{3}(|A_+|^2+\sigma|A_-|^2)A_+ =0,$$

$$i\frac{\partial A_-}{\partial Z}+i\frac{v}{2}\frac{\partial A_+}{\partial T}-\frac{k''}{2}\frac{\partial^2 A_-}{\partial T^2}+\beta A_- +\frac{\Delta\beta}{2}A_+ + \frac{2R}{3}(|A_-|^2+\sigma|A_+|^2)A_- =0, \quad (1)$$

where β and $\Delta\beta$ are the common phase velocity and the linear birefringence, v and k'' represent the walk-off between the two linear polarization modes and group velocity dispersion (this is assumed to be equal for both modes for simplicity) at the mean wavelength λ_0, respectively. Whereas R is the nonlinearity coefficient. For the purpose of analytical and numerical analysis, it is convenient to deal with a reduced number of parameters. Hence, we rewrite Eqs. (1) in terms of the dimensionless variables $u_\pm=(A_\pm/\sqrt{P})\exp(-i\beta Z)$, where $P=|A_+|^2+|A_-|^2$ is the total input pump power, obtaining

$$-i\frac{\partial u_+}{\partial \xi}=\frac{\delta H}{\delta u_+^*}=i\frac{\delta}{2}\frac{\partial u_-}{\partial \tau}-\frac{\eta}{2}\frac{\partial^2 u_+}{\partial \tau^2}+\frac{u_-}{2}+2p(|u_+|^2+\sigma|u_-|^2)u_+,$$

$$-i\frac{\partial u_-}{\partial \xi}=\frac{\delta H}{\delta u_-^*}=i\frac{\delta}{2}\frac{\partial u_+}{\partial \tau}-\frac{\eta}{2}\frac{\partial^2 u_-}{\partial \tau^2}+\frac{u_+}{2}+2p(|u_-|^2+\sigma|u_+|^2)u_-, \qquad (2)$$

where the Hamiltonian $H=\int_{-\infty}^{+\infty} d\tau\ 2p(|u_+|^4+|u_-|^4+\sigma|u_+|^2|u_+|^2)+\Sigma_{j=\pm}|u_j|^2/2-\eta|u_{j,\tau}|^2/2+\delta\ \mathrm{Re}(iu_j^*u_{j,\tau})/2$ is conserved together with the photon flux $Q=\int_{-\infty}^{+\infty}|u_+|^2+|u_-|^2\ d\tau$. In Eqs. (2) we set $\xi\equiv 2\pi Z/Z_b$, where $Z_b=2\pi/\Delta\beta$ is the linear beat length, $\tau\equiv\sqrt{2\pi/Z_b|k''|}\,T$, $\eta\equiv\mathrm{sgn}(k'')$, $\delta\equiv v/\sqrt{\Delta\beta|k''|}=(\lambda_0/2\pi c)\sqrt{\Delta\beta/|k''|}$, and $p\equiv RP/(3\Delta\beta)$ is a single parameter which has the meaning of a normalized total power. In the steady state, Eqs. (1) may be solved exactly in terms of Jacobian elliptic functions [2–5]. Such solutions are considered in detail in Appendix B.

III. BLOCH WAVE ANALYSIS

We analyzed the modulational stability of the rotating solution of Eqs. (2) by considering a small additive perturbation $a_\pm$ and linearizing the equations for $a_\pm$ about the pump. Details on the derivation of the linearized sideband equations are given in Appendix A. The linearized equations contain the formal expression of the periodic solutions for the pump fields, reported explicitly in Appendix B. The linear stability of the resulting system of four perturbation equations for the Stokes ($w_\pm$) and anti-Stokes ($v_\pm$) sidebands in each of the two counterrotating circular polarizations may be derived by applying the Floquet theory (equivalent to Bloch theory in the context of solid-state physics) of wave propagation in linear periodic media [21]. We rewrite the linearized sideband equations in the general form

$$\frac{d\mathbf{X}(\xi)}{d\xi}=\mathbf{M}(\xi)\mathbf{X}(\xi), \qquad (3)$$

where $\mathbf{X}\equiv(w_+,v_+^*,w_-,v_-^*)$, and $\mathbf{M}(\xi)$ is a ξ periodic 4×4 matrix whose spatial period $\xi\equiv\xi_B$ is equal to the nonlinear beat length or period of the stationary pump evolution from Eqs. (2) (see Appendix B). By choosing the four fundamental or independent initial conditions $\mathbf{X}_1(\xi=0)=(1,0,0,0)$, $\mathbf{X}_2(\xi=0)=(0,1,0,0)$, $\mathbf{X}_3(\xi=0)=(0,0,1,0)$, and $\mathbf{X}_4(\xi=0)=(0,0,0,1)$, one readily obtains from the solution of Eqs. (3) at $\xi=\xi_B$ the principal solution matrix $S\equiv\{X_1^t(\xi=\xi_B),X_2^t(\xi=\xi_B),X_3^t(\xi=\xi_B),X_4^t(\xi=\xi_B)\}$ (here t denotes the vector or matrix transpose). By applying Floquet (or Bloch) theorem [21], the eigenvalues $\lambda\equiv\exp(\eta_F+i\sigma)$ of S (these are also known as Floquet multipliers) such that $|\lambda|>1$ yield the linear instability of the pump wave with respect to the growth of sidebands with a given frequency detuning, say, Ω. In fact, the scattering matrix at an integer number of periods, say $\xi=n\xi_B$, is S^n. In the special case where the pump is coupled to a stable fiber principal axis, $|\lambda|=\exp(\eta_F)$ and $G=2\eta_F/\xi_B$ reduces to the usual MI power gain, where ξ_B represents the period of small polarization oscillations about this axis.

IV. MODULATIONAL GAIN SPECTRA

As we have seen, the Floquet theorem permits us to numerically calculate from the Floquet exponent η_F the unstable sideband power gain (or growth rate) $G\equiv 2\ \ln|\lambda|/\xi_B$, as a function of the sideband detuning Ω and the dimensionless pump power p. The condition $p=0.5$ corresponds to the bifurcation of the fast axis eigenmode, whereas $p=1$ corresponds to the cw switching power for a circular pump [19]. For simplicity, we restrict our attention here to the case of normal group velocity dispersion (i.e., $\eta=-1$), and we mainly consider the case of a weakly birefringent fiber, that is, where it is reasonable to neglect the polarization walk-off. However, we briefly discuss the effect of varying the polarization dispersion δ in the most relevant case of a pump equally split between the two birefringence axes. In the anomalous dispersion regime, the usual scalar MI has typically larger gain values than the polarization instability and therefore polarization effects are more difficult to observe. Moreover, the numerical solutions indicate that the competition between scalar and perpendicular modulational instabilities lead to spatiotemporal chaotic behavior for the light waves in birefringent fiber [12].

First of all, it is interesting to compare the (analytical) modulational gain spectra that are obtained when the pump wave is oriented exactly on the polarization eigenmodes (i.e., either the fast or the slow birefringence axis) of the cw solutions of Eqs. (1), with the Floquet gain spectra which correspond to a pump that is initially very close to the same eigenmodes. In Fig. 1, the solid curves indicate the MI gain G versus the sideband detuning Ω with a linearly polarized pump wave that is oriented either at 1° from the slow [Fig. 1(a)] or the fast [Fig. 1(b)] axis. Here the dimensionless pump power $p=1.2$. On the other hand, the dashed curves in Fig. 1 show the conventional MI gain G_a that is predicted with a pump that is coupled exactly on either the slow or the fast axis [9]. This gain reads as

$$G_a=\sqrt{(\Omega^2\mp2)(4p-\Omega^2\pm2)}\ , \qquad (4)$$

where the upper (lower) signs stand for a pump aligned with the slow (fast) fiber axis.

As can be seen in Fig. 1, in the case of slow axis excitation, the parametric gain curve is virtually the same whenever the pump is rotated from the axis by a few degrees. Whereas Fig. 1(b) reveals that the shape of the MI spectrum with the pump on the cw unstable fast axis may be deeply deformed as soon as the pump wave is slightly misaligned from the axis. In particular, the MI gain with a finite detuning from the pump (e.g., for $\Omega\simeq1$) takes much larger values than the gain at zero detunings, which corresponds to the cw polarization instability effect. In such cases, the noise-seeded MI will preferably lead to the growth of sidebands with relatively large detunings, with either slow or fast axis excitation. The sensitivity of the gain shape to small changes of the input polarization of the pump, when this is aligned with the

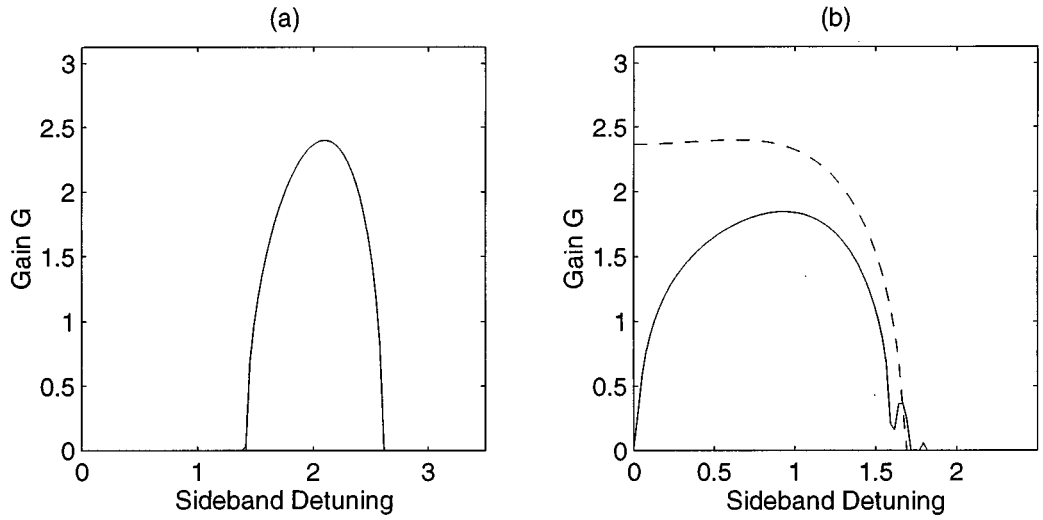

FIG. 1. The solid curves indicate the MI gain G vs sideband detuning Ω for $p=1.2$ and a linearly polarized pump wave oriented at 1° from the (a) slow axis or (b) fast axis. The dashed curve in (b) shows the on-axis gain G_a.

fast axis, is clearly associated with the cw instability of this eigenmode (which corresponds to an unstable saddle point in the phase-space representation). In fact, as shown in Fig. 2(a), for a pump wave that is initially polarized close to the slow mode the state of polarization executes small oscillations about this stable axis. On the other hand, Fig. 2(b) shows that for $p\simeq 1$, even the slightest misalignment from the fast axis leads to large periodic polarization rotations that approach counterrotating circular states. In Fig. 2 we display the evolution of the polarization angle [relative to the slow and fast axis in Fig. 2(a) and Fig. 2(b), respectively] versus the ellipticity $e\equiv|A_+|^2-|A_-|^2$ over the nonlinear beat length ξ_B. Here the pump with power $p=1$ is linearly polarized at the input, and it is oriented at 1° from either the slow [Fig. 2(a)], or the fast [Fig. 2(b)] fiber axis.

Figure 3 illustrates dependence on input power p of the shape of the Floquet gain spectrum with a pump at 1° from the fast axis as in Fig. 1. As can be seen in Fig. 3(b), only in the case with $p=1$ the gain shape of the eigenmode is nearly preserved. Whereas for pump-power values that are about 10% lower or higher than unity, the modulational gain at zero detunings drops to low values and peak gain is obtained at a finite sideband frequency shift [see Fig. 3(a) with $p=0.75$, Fig. 3(c) with $p=1.5$, and Fig. 3(d) with $p=2$]. For pump powers lower than the cw polarization instability threshold $p=0.5$, no MI is observed as the pump is polarized close to the fast axis. We may, therefore, conclude that the large asymmetry between fast and slow axes, which exists in the cw evolutions [6] and in the gain spectra for a pump exactly aligned with an axis [9], is not preserved for a small misalignment. This explains the inherent practical difficulty in observing the fast axis instability in the experiments [20].

Clearly, the Floquet analysis may perfectly apply to calculate the modulational gain spectra that are associated with any periodic evolution of the pump beam. For example, Fig. 4 illustrates the dependence of the sideband gain G on the

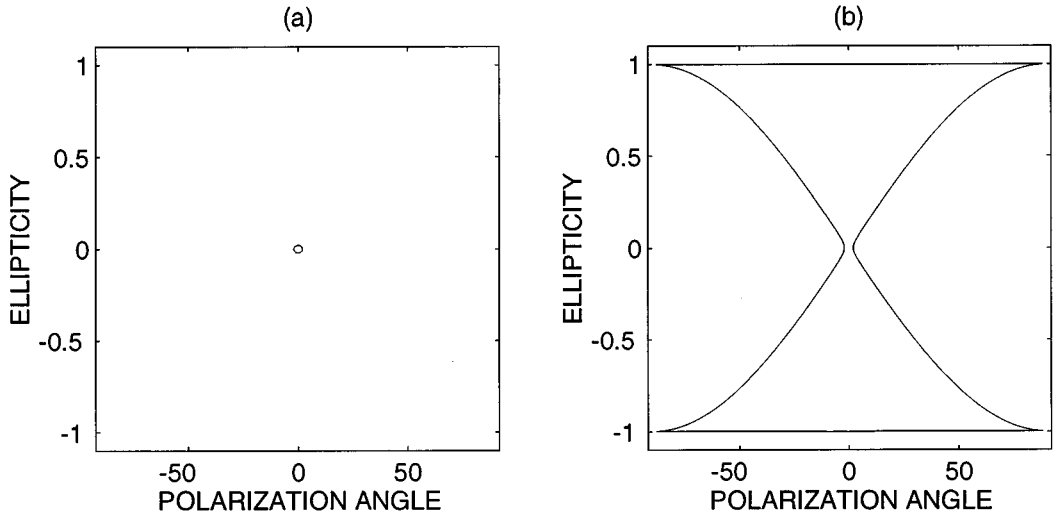

FIG. 2. Phase-space representation of pump polarization evolution over the period ξ_B, for an input linear polarization at angle $\theta=1°$ from (a) slow or (b) fast fiber axis.

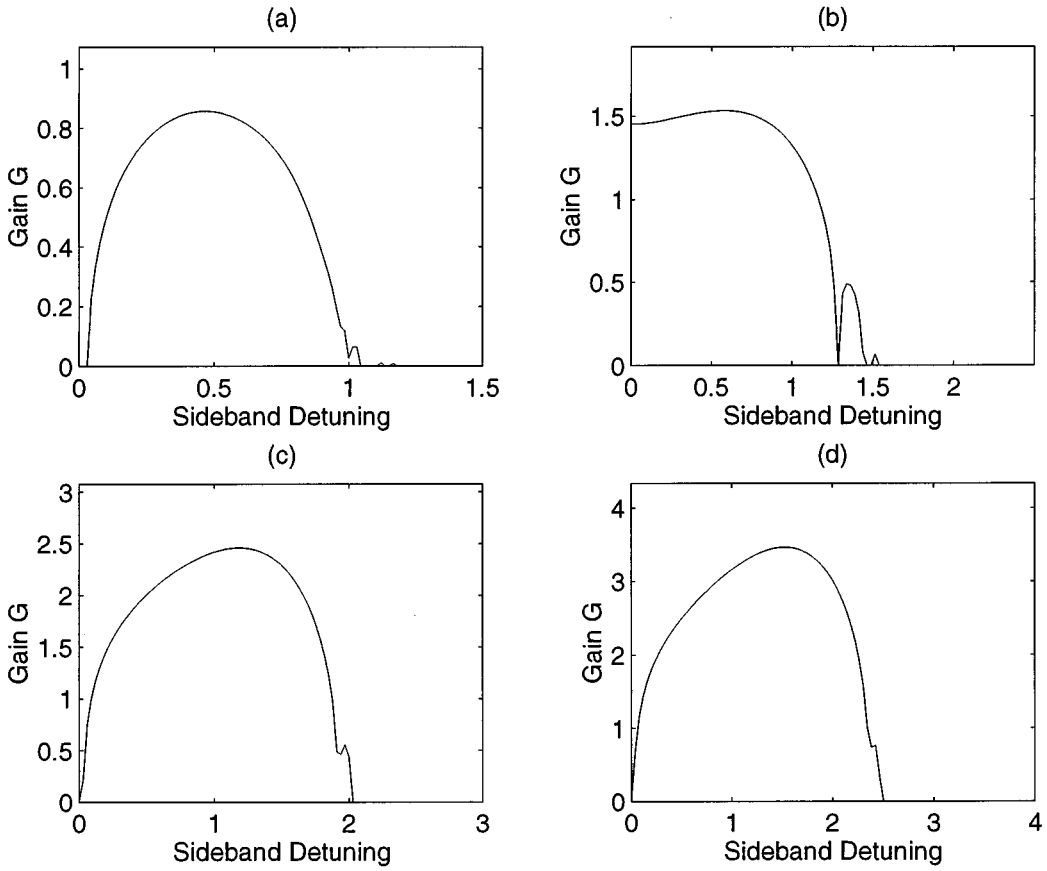

FIG. 3. As in Fig. 1, with a pump at 1° from the fast axis, and (a) $p=0.75$, (b) $p=1$, (c) $p=1.5$, and (d) $p=2$.

input power p, with a pump at 45° from the birefringence axes. This permits to extend to the case of low or intermediate birefringence, the analysis that was previously carried out only in the high-birefringence limit [14,15]. In Fig. 4 we show the limit case $\delta=0$. As it can be seen, in this case MI is present (with a reduced gain) also for relatively low pump powers: Fig. 4(a) has been obtained for $p=0.25$, and shows the presence of multiple narrow gain peaks for sideband shifts slightly larger than unity. On the other hand, Figs. 4(b)–4(c) show that for $p\geqslant 0.5$ the MI gain curve has a single peak at progressively larger detunings, similar to the case when the slow axis is excited.

Let us briefly consider now the role of finite polarization dispersion δ on the MI spectra with a pump at 45° between the axes. By using the relationship $\delta=(\lambda_0/2\pi c)\sqrt{2\pi}/(Z_B|k''|)$, in the case of a high-birefringence fiber with $Z_B=1.25$ mm (as in Ref. [15], where the group-velocity walk-off was equal to $v=1.6$ ps/m at $\lambda_0=600$ nm) and the group-velocity dispersion $k''=65\ \mathrm{ps}^2/\mathrm{km}$, one obtains the relatively small value $\delta\simeq 0.09$. The gain spectra calculated for the same power values as in Fig. 4 show that little changes occur with respect to the $\delta=0$ case in this range of values of group-velocity difference (and even for one order of magnitude larger walk-off, equivalent to linear beat lengths ten times shorter than the value of the experiment in Ref. [15]). We may, therefore, conclude that polarization dispersion does not influence polarization instabilties in optical fibers at operating wavelengths is the visible region of the spectrum.

On the other hand, for beam propagation close to the zero-dispersion wavelength region, the relative importance of polarization walk-off increases and, as a result, a superposition may occur between the modulational gain spectra that originate from different mechanisms of phase matching. Considering, for example, the case with $Z_B=1.25$ mm, $\lambda_0=1.55$ μm, and $k''=0.4\ \mathrm{ps}^2/\mathrm{km}$, one obtains $\delta\simeq 2.8$. Figure 5 has been obtained in this case: as can be seen, for $p<1$ the main feature of these spectra is the appearance of a large number of gain peaks for sideband detunings $\Omega<\Omega_l$, where $\Omega_l=\delta$ corresponds to the low-power limit of the phase-matching condition of four-wave mixing in a high-birefringence fiber [15]. Nevertheless, Figs. 5(c) and 5(d) show that for power values p equal or larger than one, the gain spectral profile of coherent MI is still nearly unchanged with respect to the $\delta=0$ case.

Another interesting example of application of the Floquet-Bloch analysis is the computation of the gain spectra when the pump is circularly polarized. This input condition corresponds to the case that was considered in the early experiments of polarization instability in birefringent fibers [19]. Note that this situation directly corresponds to the input excitation of an individual guide when Eqs. (1) describe the waveguide field coupling in a nonlinear directional coupler. Figure 6 shows that cw gain (i.e., at $\Omega=0$) is observed in this case as long as $p\leqslant 1.5$. Figure 6(a) ($p=0.75$) and Fig. 6(b) ($p=1.01$) show that for $p\leqslant 1$ the MI gain profile is spectrally flat, whereas the cutoff frequency grows larger with input power. Whereas for $p\geqslant 1.5$ [see Fig. 6(c)] the cw

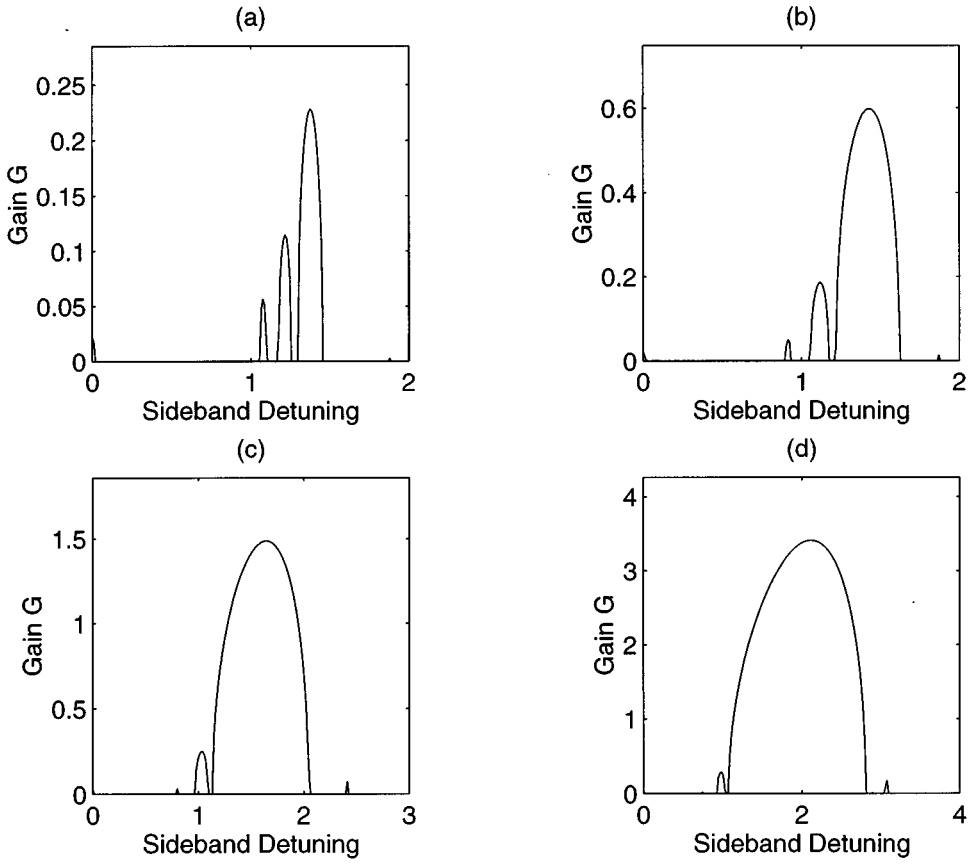

FIG. 4. As in Fig. 3, with a pump at 45° from fiber axes, $\delta=0$ and (a) $p=0.25$, (b) $p=0.5$, (c) $p=1$, and (d) $p=2$.

gain starts to drop relative to the peak value at finite detunings. Finally, Fig. 6(d) shows that for $p=2$ the gain spectrum exhibits a single peak at progressively larger values of the frequency shift.

V. NUMERICAL RESULTS

In this section, we compare the predictions of the linear stability analysis with the full numerical solutions of Eqs. (2). In order to simulate either the induced or the spontaneous MI, we shall consider as initial condition to the simulations, the injection along with the pump beam of either a pair of sidebands perturbation [i.e., $a_{\pm}=\epsilon\cos(\Omega\tau)$ where typically we take ϵ in the range between $\epsilon=10^{-4}$ and $\epsilon=10^{-6}$] or Gaussian-distributed white noise, respectively. For the numerical solution of Eqs. (2) we used the standard Fourier split-step (or beam propagation) method where periodic boundary conditions are implicitly imposed. We use a typical mesh of 1024 points on a temporal window which is typically four times the period of the unstable modulation. This ensures that the spectral window includes several higher-order sidebands of the injected (or most unstable) perturbation (in the figures reported below, we show only the central region of the spectral window). The envelope amplitudes of the linearly polarized components along the slow and fast axes are obtained as $u_x=(u_++u_-)/\sqrt{2}$ and $u_y=i(u_--u_+)/\sqrt{2}$, respectively.

Figure 7 shows the evolution for a distance $\xi=3\xi_B$ of the slow axis component of the field intensity. The linearly polarized pump with power $p=1$ is oriented at 1° from the (stable for cw) slow axis of the fiber. The MI is induced by seeding the pump beam with weak upshifted and downshifted sideband pair at frequency given by the optimal (i.e., yielding the peak gain) detuning $\Omega\equiv\Omega_p\simeq 2$. As shown in the first stage of propagation, the pump wave remains polarized very close to the slow axis [note that the uniform polarization rotation shown in Fig. 2(a) is too small to be seen in Fig. 7]. However, after about one linear beat length (i.e., $\xi=2\pi$) a deep temporal modulation develops on both polarizations. At the same distance, a strong temporal modulation also develops over the weak fast axis component (not shown in Fig. 7).

The frequency content of this modulation is clearly illustrated in Fig. 8, that shows the spectral intensity of both polarization field components. It is evident that the MI of the pump leads to nearly complete depolarization of the input beam through the decay into its sideband modes and their harmonics. These periodically oscillating sidebands have indeed a strong component along the fast axis.

In Fig. 9 we show the spectral evolution of the polarization components when the seed frequency is chosen outside the gain bandwidth (e.g., $\Omega=1$ in this case). The contrast with the case of Fig. 8 is clear. In this case, the small cw polarization rotation dominates the evolution of the input beam, and an extremely weak conversion (notice the different vertical scale for the fast mode in Fig. 8 and Fig. 9) is visible only after three nonlinear beat length.

The nonlinear development of MI for a pump wave po-

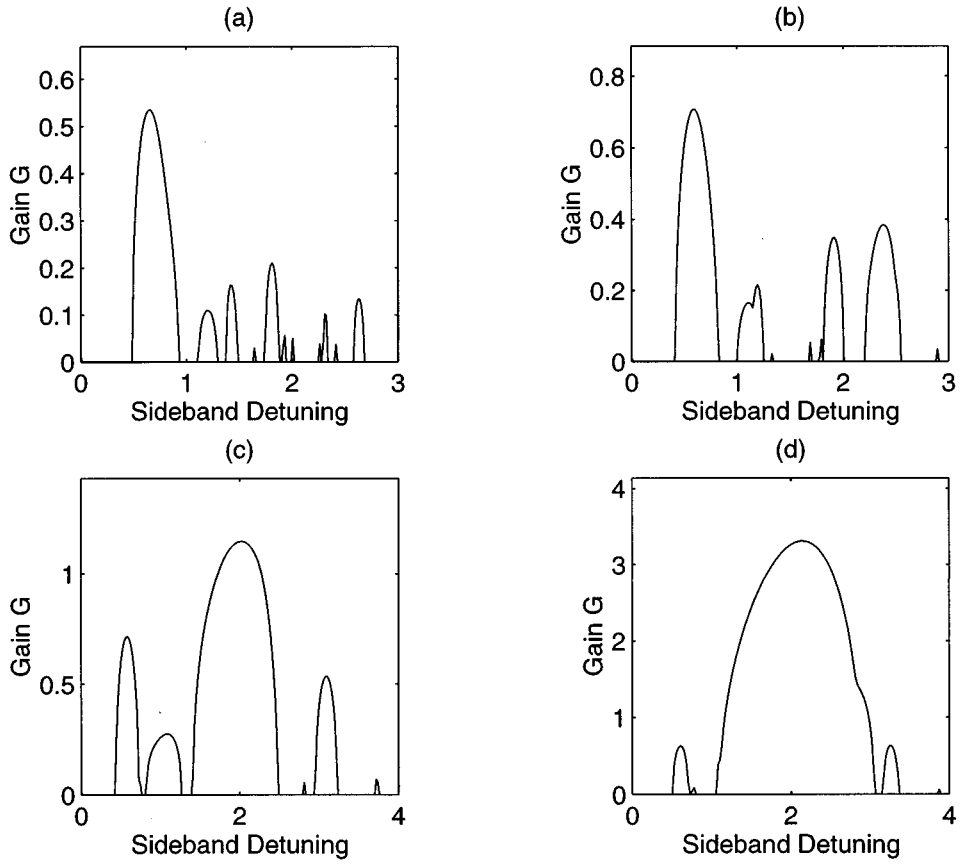

FIG. 5. Same as in Fig. 4, with $\delta = 2.8$.

larized close to the (cw unstable) fast fiber axis is shown in Fig. 10 for one period (i.e., nonlinear beat length $\xi = \xi_B \simeq 19$) of the evolution. Here we display the evolution of the spectral components of the light field in the slow and fast polarization modes, when the pump beam is oriented at 1° from the fast axis, and $p = 1$. Again, the MI is induced by sidebands with $\Omega = \Omega_p \simeq 1$. In this case, the cw instability of the pump initially leads to its almost complete rotation into the orthogonal slow mode. Remind that this conversion occurs twice within one period [see Fig. 2(b)]. However, after the initial conversion is ultimated, when back conversion from the slow into the fast mode sets in, one observes the onset of parametric scattering into the sideband modes. Note that the polarization sidebands develop at nearly the same distance in the case of either slow (see Fig. 8) or fast (see Fig. 10) mode excitation. These results clearly confirm that, due to parametric conversion or MIs, the asymmetry between fast and slow modes which is predicted by the cw analysis is a transient effect which only lasts over about one linear beat lengths (i.e., $\xi \simeq 2\pi$). Beyond this distance, an intense monochromatic pump wave decays into a set of sidebands with periodically rotating states of polarization, nearly irrespective of the choice of the input polarization angle (i.e., close to either the slow or fast axis).

In the case of spontaneous (i.e., noise seeded) MI, the decay of the dynamically evolving cw pump occurs in favor of the amplification of a range of frequencies that lie within the gain spectrum. For example, we simulated the spontaneous parametric decay of an intense pump wave with a dimensionless power $p = 1$, that was linearly polarized at 1° from either the slow or fast axis, respectively. With a pump close to the slow axis one observes the buildup of side frequencies polarized along the fast axis and peaked around the peak frequency detuning $\Omega = 2$, in agreement with the relatively narrowband parametric gain spectrum [see Fig. 1(a)]. Conversely, one obtains that a pump polarized close to the fast axis decays through the emission of a broadband spectrum of side modes, which corresponds to the complete depolarization of the input field.

At low power the parametric decay has a lower gain, and is expected to occur on a longer scale length, that is after several spatial periods of polarization rotation of the pump. This is shown in Fig. 11, where we report the evolution of the slow axis intensity, for a pump beam polarized at 20° from the slow axis $p = 0.3$ [here the peak gain is $G = G(\Omega_p) \simeq 0.5$], and injected sidebands at $\Omega = \Omega_p = 1.57$. As shown, in this case the depolarization of the cw beam accompanied by the parametric decay only occurs after several cycles of polarization oscillation.

Finally, we also simulated the evolution of a circularly polarized pump beam at the input. In this case the most interesting behavior occurs around the critical power $p = 1$. At powers slightly below $p = 1$ a cw pump experiences complete polarization rotations, whereas above $p = 1$ the pump only exhibits relatively small oscillations about the input circular polarization [6,7]. Moreover, crossing the critical condition $p = 1$ leads to halving the spatial period ξ_B (e.g., for

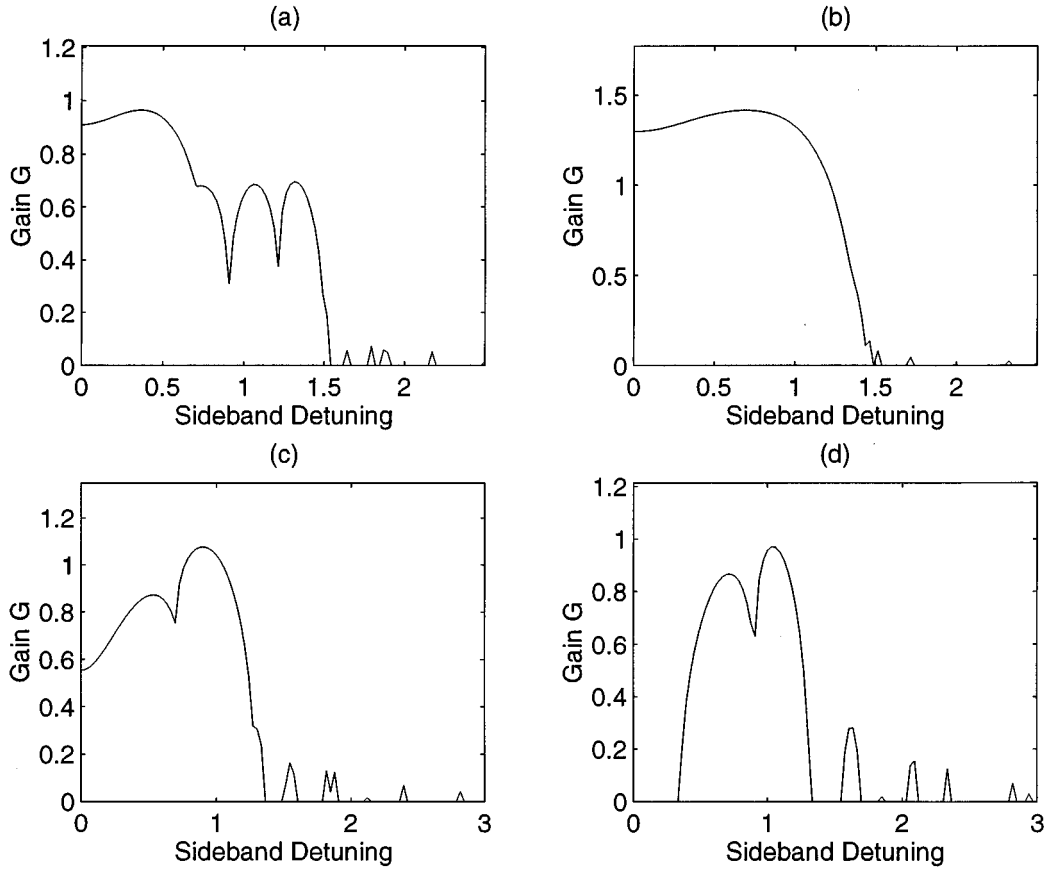

FIG. 6. As in Fig. 3, with a circularly polarized pump wave, and (a) $p=0.75$, (b) $p=1.01$, (c) $p=1.5$, and (d) $p=2$.

$p=0.99$ and $p=1.01$ we obtain $\xi_B=13.4$ and $\xi_B=6.7$, respectively; see also Appendix B). However, our present results show that the decay of the periodically coupled polarization modes via MI poses a limitation to the distance for which this cw picture describes accurately the propagation dynamics. After one or few (depending slightly on the initial seed) spatial periods of the pump polarization rotation, an injected or spontaneously growing periodic modulation draws a significant amount of energy from the rotating pump waves. This modulation rapidly develops into a series of higher-order harmonics which lead to an irregular beating of the field intensity profile. Figure 12 shows the evolution of the spectral intensities in the right-handed and left-handed circular modes, for an initially left-handed pump of power $p=1.01$, and white-noise seeding. As shown, the pump beam experiences cw conversion over one complete period ($\xi\simeq 7$), after which the long-range evolution (in the figure, we show the evolution over the distance $\xi\simeq 2\xi_B$) is dominated by a strong decay into sideband modes, which in turn is responsible for the depolarization of the pump beam. In the formally equivalent case of a nonlinear directional coupler [1], this phenomenon of parametric scattering into sidebands is expected when cw (or quasi-cw) light is coupled into an individual guide of a beam with power slightly above the switching power of the coupler. A parametric decay is also obtained over comparable distances in the simulations with pump powers slightly below the critical power $p=1$ (e.g., with $p=0.99$).

The above simulation results that were obtained with a circularly polarized pump mode clearly demonstrate the limit of validity of the purely cw (or dispersionless) description of polarization instabilities in birefringent nonlinear optical media. In fact, when dispersion (and thus phase matching involving other frequency components) is taken into account, one observes that the cw period doubling phenomenon and the abrupt polarization switching, which are both associated with the crossing of the cw critical switching power $p=1$ are

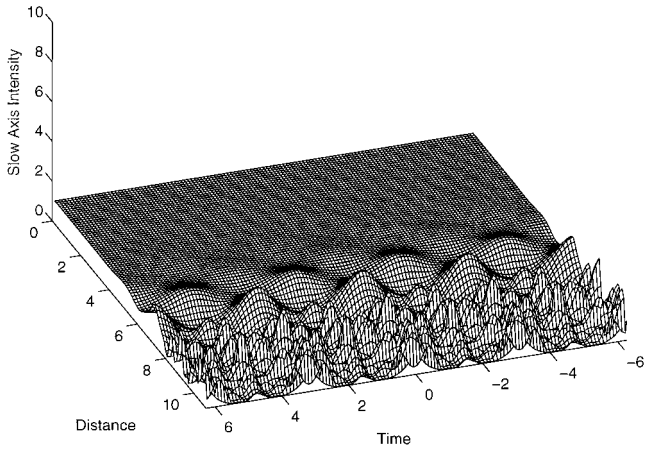

FIG. 7. Evolution of normalized intensity in the slow mode vs distance ξ and time τ. Here the pump is launched with linear polarization at 1° from slow axis, $p=1$, and the seed frequency detuning is $\Omega=\Omega_p=2$.

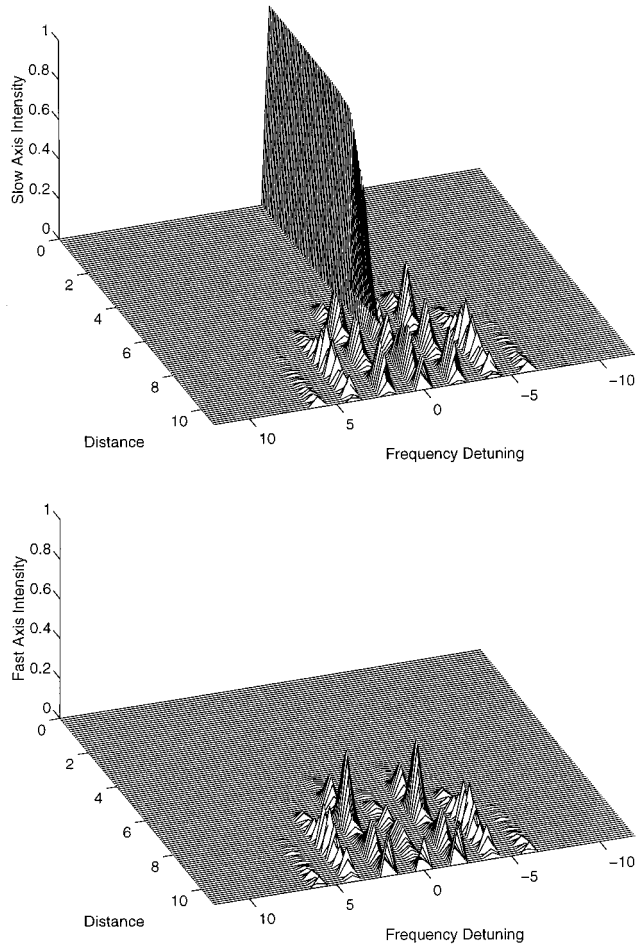

FIG. 8. Evolution of spectral intensity fractions in the slow and fast modes vs distance ξ and frequency detuning Ω, and input at $\zeta=0$ as in Fig. 7.

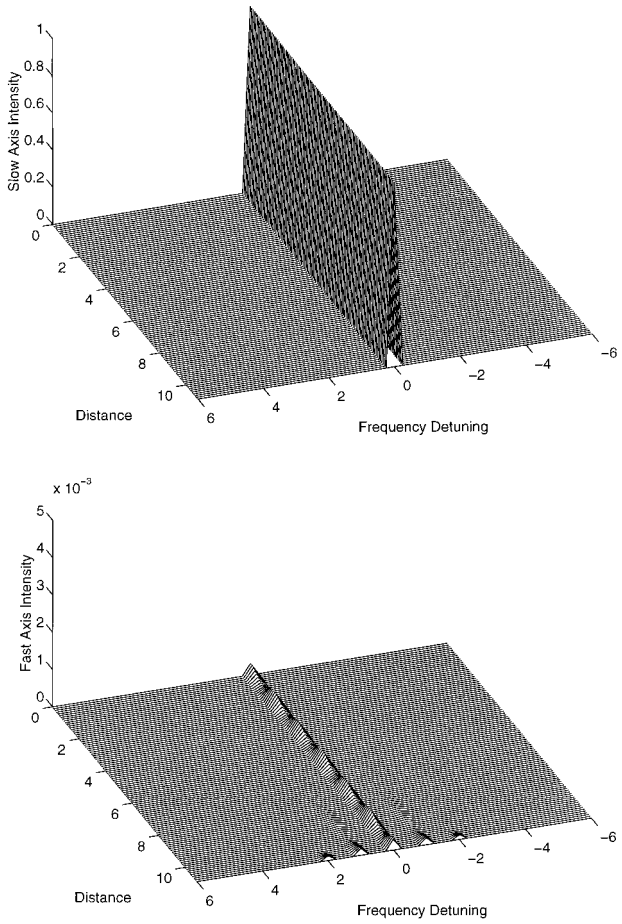

FIG. 9. As in Fig. 8 for a seed frequency detuning $\Omega=1$, outside the gain bandwidth.

physically observable only for relatively short propagation distances (i.e., about one or two linear beat lengths). To the contrary, for longer interaction distances the present analysis reveals that parametric decay or MI leads to a substantial scattering of energy into a series of sidebands of different polarizations and frequencies.

VI. CONCLUSIONS

In this work, we extended the theory of modulational polarization instabilities in birefringent nonlinear fibers to the case of an arbitrarily polarized pump beam. The nonlinear polarization rotation of the pump is taken into account by means of the available exact solutions in terms of Jacobian elliptic functions. The stability of two pairs of weak sidebands on each birefringence axis was then investigated by means of Floquet-Bloch theorem. The gain spectra have then been computed for different initial pump orientations and power values. The analysis has revealed that the modulational gain spectra that are obtained with a pump beam oriented along the unstable fast axis may strongly distort their shape when the pump is slightly misaligned from that axis. In particular, the large amplitude periodic rotation of the pump polarization generally leads to prevailing growth of modulational (i.e., with a relatively large frequency offset from the pump) rather than quasi-cw perturbations. This points to a fundamental difficulty in the experimental observation of the asymmetry between the two axes which is predicted by the cw theory of polarization instability. We confirmed the validity of the linearized theory predictions by means of the comparison with the direct solution of the coupled nonlinear Schrödinger equations that describe beam propagation in the birefringent fiber.

Note that the same technique that we used here also permits the study of the polarization stability of a weak signal in the presence of a counterpropagating intense pump in the birefringent fiber [22]. Finally, we point out that the spatial counterpart of the present phenomenon is expected to give rise to the filamentation of periodically coupled polarization plane waves (i.e., dynamical transverse MI).

ACKNOWLEDGMENTS

We acknowledge stimulating discussions with E. A. Golovchenko and A. N. Pilipetskii on the calculation of modulational polarization instability gain spectra with a rotating pump wave. We also thank R. Chisari for her patient technical assistance. This work was carried out in the framework of the agreement between Fondazione Ugo Bordoni and the Italian Post and Telecommunications Administration.

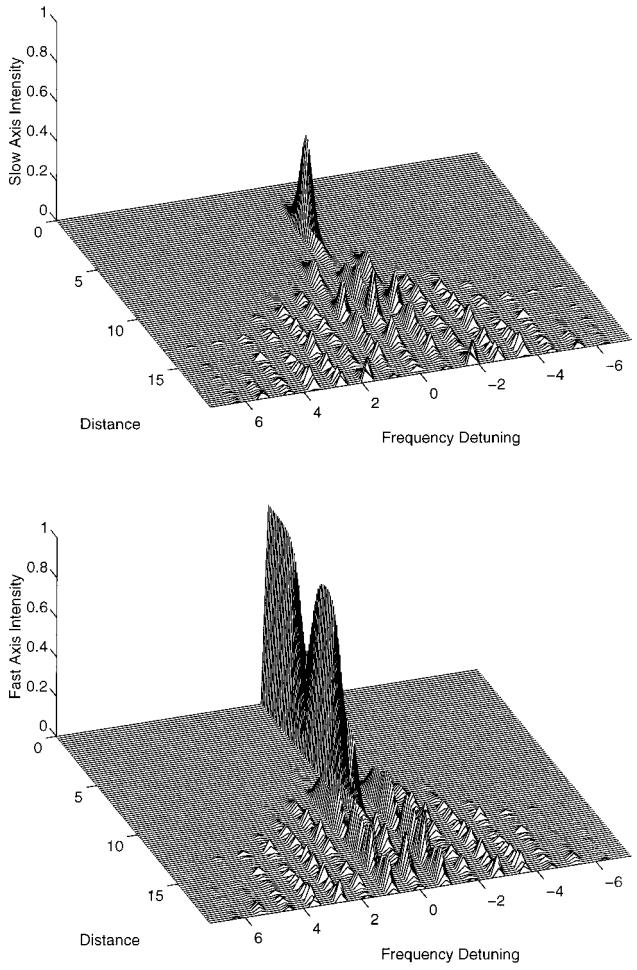

FIG. 10. As in Fig. 8 for an input pump polarization at 1° from the fast axis, $p=1$, and a seed frequency detuning $\Omega=\Omega_p\simeq 1$.

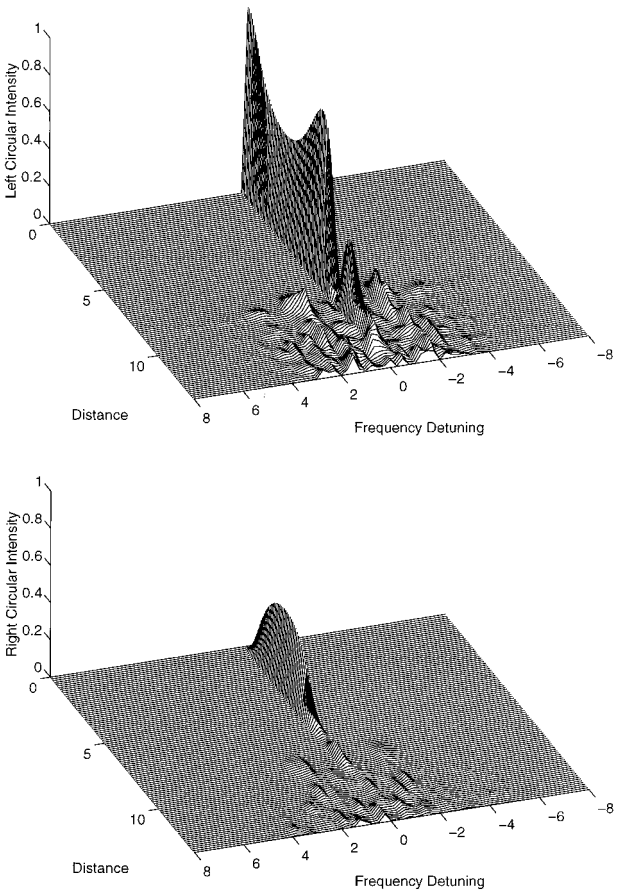

FIG. 12. Spectral intensity in the circular modes, for a left-handed input with $p=1.01$, and white-noise seeding.

APPENDIX A: LINEARIZED EQUATIONS

In this Appendix, we present the derivation of the coupled linearized equations for the four sideband amplitudes in the two orthogonal circular polarization components of the pump wave. We express the pump fields at central frequency in terms of modulus and phase as $u_\pm \equiv \overline{u}_\pm(\xi) = |A_\pm| \exp\{i\psi_\pm\}$. The perturbed pump field reads as

$$u_\pm = (|A_\pm| + a_\pm)\exp(i\psi_\pm) \ , \tag{A1}$$

where $|a_\pm| \ll |A_\pm|$. Let us neglect, at first, the time dependence of the fields. Inserting Eq. (A1) into Eqs. (2) yields

$$-i\frac{\partial a_+}{\partial \xi} = -a_+\frac{\partial \psi_+}{\partial \xi} + \frac{a_-}{2}e^{-i\phi} + 2p\sigma|A_+||A_-|(a_- + a_-^*) + 2p[(2|A_+|^2 + \sigma|A_-|^2)a_+ + |A_+|^2 a_+^*] \ ,$$

$$-i\frac{\partial a_-}{\partial \xi} = -a_-\frac{\partial \psi_-}{\partial \xi} + \frac{a_+}{2}e^{i\phi} + 2p\sigma|A_+||A_-|(a_+ + a_+^*) + 2p[(2|A_-|^2 + \sigma|A_+|^2)a_- + |A_-|^2 a_-^*] \ , \tag{A2}$$

where the modulus $|A_\pm|$ and phase $\psi_\pm$ of the unperturbed fields obey the following equations obtained from Eqs. (2):

$$\frac{\partial |A_\pm|}{\partial \xi} = \pm\frac{|A_\mp|}{2}\sin\phi \ , \tag{A3}$$

$$\frac{\partial \psi_\pm}{\partial \xi} = 2p(|A_\pm|^2 + \sigma|A_\mp|^2) + \frac{|A_\mp|}{2|A_\pm|}\cos\phi \ , \tag{A4}$$

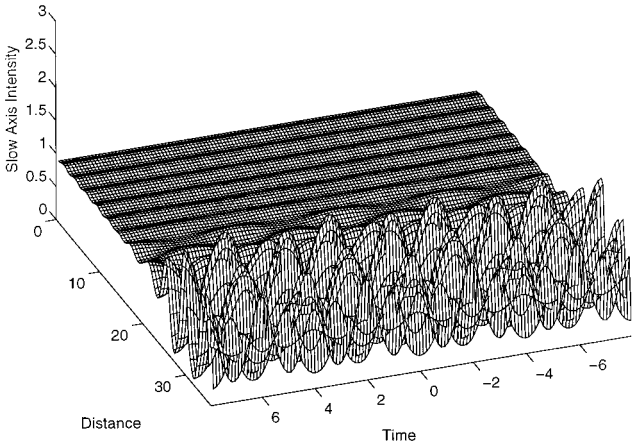

FIG. 11. As in Fig. 7, for a pump at 20° degree from slow axis, $p=0.3$ and $\Omega=\Omega_p=1.57$.

and $\phi \equiv \psi_+ - \psi_-$ is a nonlinear phase shift, which is responsible for the power-dependent ellipse rotation of the pump wave. For silica fibers, that is, for $\sigma = 2$, Eq. (A4) becomes

$$\frac{\partial \psi_\pm}{\partial \xi} = 3p + p(|A_\mp|^2 - |A_\pm|^2) + \frac{|A_+||A_-|}{2|A_\pm|^2}\cos\phi \ , \tag{A5}$$

whereas the phase shift ϕ obeys

$$\frac{\partial \phi}{\partial \xi} = \frac{|A_-|^2 - |A_+|^2}{2|A_-||A_+|}\cos\phi - 2p(|A_+|^2 - |A_-|^2). \tag{A6}$$

The pump wave evolution [i.e., the solution of Eqs. (A3) and (A4)] can be expressed more easily either by means of a Hamiltonian reduction to a one-dimensional oscillator [8], or with the help of the Stokes parameters [5,6]. Both methods permit the representation of the propagation evolution in a properly defined phase space. Here we choose the latter description, introducing the dimensionless Stokes parameters s_i, $i = 1,2,3$,

$$\begin{aligned} s_1 &= 2|A_+||A_-|\cos\phi \ , \\ s_2 &= 2|A_+||A_-|\sin\phi \ , \\ s_3 &= |A_-|^2 - |A_+|^2 \ , \end{aligned} \tag{A7}$$

that represent the local state of polarization of the pump. In fact, the analytical solution for the evolution of the Stokes vector $\mathbf{s} = (s_1, s_2, s_3)$ is easily written in terms of simple expressions involving Jacobian elliptic functions (see Appendix B). Equation (A5) is easily reexpressed as

$$\frac{\partial \psi_\pm}{\partial \xi} = 3p \pm p s_3 + \frac{s_1}{2(1 \mp s_3)} \ , \tag{A8}$$

and, after substitution in Eq. (A2), yields

$$\begin{aligned} -i\frac{\partial a_+}{\partial \xi} = &\left[p(1-s_3) - \frac{1}{2}\frac{s_1}{(1-s_3)} \right] a_+ + p(1-s_3)a_+^* \\ &+ \left(\frac{s_1 - i s_2}{2\sqrt{1-s_3^2}} + 2p\sqrt{1-s_3^2} \right) a_- + 2p\sqrt{1-s_3^2}\, a_-^* \ . \end{aligned} \tag{A9}$$

The equation for a_- is simply obtained from Eq. (A9) by changing the sign of s_2 and s_3. The time dependence of the perturbing fields $a_\pm$ is now reintroduced, and we write the perturbation as the sum of Stokes and anti-Stokes (i.e., frequency down and up shifted by, say, $\Omega > 0$) sidebands with amplitudes $w_\pm$ and $v_\pm$, respectively: $a_\pm \equiv a_\pm(\xi, T) = w_\pm(\xi)\exp(i\Omega\tau) + v_\pm(\xi)\exp(-i\Omega\tau)$. The resulting coupled equations for w_+ and v_-^* read as

$$\begin{aligned} -i\frac{\partial w_+}{\partial \xi} = &\left[\frac{\eta}{2}\Omega^2 + p(1-s_3) - \frac{1}{2}\frac{s_1}{(1-s_3)} \right] w_+ \\ &+ p(1-s_3)v_+^* + 2p\sqrt{1-s_3^2}\, v_-^* \\ &+ \left(\frac{s_1 - i s_2}{2\sqrt{1-s_3^2}} + 2p\sqrt{1-s_3^2} + \Omega\delta \right) w_- \ , \\ -i\frac{\partial v_+^*}{\partial \xi} = &-\left[\frac{\eta}{2}\Omega^2 + p(1-s_3) - \frac{1}{2}\frac{s_1}{(1-s_3)} \right] v_+^* \\ &- p(1-s_3)w_+ - 2p\sqrt{1-s_3^2}\, w_- \\ &- \left(\frac{s_1 + i s_2}{2\sqrt{1-s_3^2}} + 2p\sqrt{1-s_3^2} - \Omega\delta \right) v_-^* \ . \end{aligned} \tag{A10}$$

Equations (A10) are coupled to analogous equations for w_- and v_-^*, which are simply obtained by exchanging the plus and minus subscripts as well as the sign of s_2 and s_3 in Eqs. (A10). These four equations can be rearranged to yield Eq. (3) for the vector $\mathbf{X} \equiv (w_+, v_+^*, w_-, v_-^*)$.

APPENDIX B: EXACT SOLUTIONS FOR THE PUMP FIELDS

In this appendix, we present the exact solutions for the periodically rotating pump wave in terms of the Stokes parameters (A7). Equations (2) with $\partial/\partial\tau \equiv 0$ immediately yield the equations for the Stokes parameters

$$\dot{s}_1 = 2p s_2 s_3, \quad \dot{s}_2 = -2p s_1 s_3 - s_3, \quad \dot{s}_3 = s_2, \tag{B1}$$

where the dot stands for derivation with respect to ξ. With a linearly polarized pump, initially oriented at an angle θ with respect to the slow axis of the birefringent fiber, one obtains [3]

$$\begin{aligned} s_1(\xi) &= \cos(2\theta) + p\ \sin^2(2\theta)\frac{\mathrm{sn}^2(f\xi;m)}{f^2\,\mathrm{dn}^2(f\xi;m)} \ , \\ s_2(\xi) &= \sin(2\theta)\frac{\mathrm{cn}(f\xi;m)}{\mathrm{dn}^2(f\xi;m)} \ , \\ s_3(\xi) &= -\ \sin(2\theta)\frac{\mathrm{sn}(f\xi;m)}{f\,\mathrm{dn}(f\xi;m)} \ , \end{aligned} \tag{B2}$$

where

$$\begin{aligned} f &= [1 + 4p^2 + 4p\ \cos(2\theta)]^{1/4} \ , \\ m &= \frac{1}{2}\left[1 - \frac{1 + 2p\ \cos(2\theta)}{f^2} \right] . \end{aligned} \tag{B3}$$

Note that m is the Jacobian parameter, not the modulus $k \equiv \sqrt{m}$.

In the case of a circularly polarized pump wave, for $p < 1$

$$s_1(\xi) = -p\ \mathrm{sn}^2(\xi;m)\ ,$$
$$s_2(\xi) = \mp \mathrm{sn}(\xi;m)\mathrm{dn}(\xi;m)\ , \tag{B4}$$
$$s_3(\xi) = \pm \mathrm{cn}(\xi;m),$$

with $m=p^2$. For $p>1$

$$s_1(\xi) = -p^{-1}\mathrm{sn}^2(p\xi;m)\ ,$$
$$s_2(\xi) = \mp p^{-1}\mathrm{sn}(p\xi;m)\mathrm{cn}(p\xi;m)\ , \tag{B5}$$
$$s_3(\xi) = \pm \mathrm{dn}(p\xi;m),$$

with $m=p^{-2}$. Finally, for $p=1$

$$s_1(\xi) = -\tanh^2(\xi)\ ,$$
$$s_2(\xi) = \mp \tanh(\xi)\mathrm{sech}(\xi)\ , \tag{B6}$$
$$s_3(\xi) = \pm \mathrm{sech}(\xi).$$

For input linearly polarized pumps, the spatial period ξ_B (in real-world units the period becomes $Z_B=\xi_B Z_b/2\pi$) of the nonlinear pump polarization rotation read as

$$\xi_B = \frac{4K(m)}{f}\ , \tag{B7}$$

where K is the complete elliptic integral of the first kind. Whereas with a circular pump, the above expression (B7) remains valid for $p<1$, with $f=1$, and $m=p^2$. Above critical power ($p>1$), the spatial period becomes

$$\xi_B = \frac{2K(m)}{p}\ , \tag{B8}$$

with $m=p^{-2}$. Clearly, the period $\xi_B\to\infty$ for $p=1$, and doubles as the critical value $p=1$ is crossed.

[1] S. Jensen, IEEE J. Quantum Electron. **QE-18**, 1580 (1982).
[2] W. Gadomsky and M. Roman, Opt. Commun. **33**, 331 (1980).
[3] K. Sala, Phys. Rev. A **29**, 1944 (1984).
[4] H. G. Winful, Appl. Phys. Lett. **47**, 213 (1985).
[5] B. Daino, G. Gregori, and S. Wabnitz, J. Appl. Phys. **58**, 4512 (1985).
[6] B. Daino, G. Gregori, and S. Wabnitz, Opt. Lett. **11**, 42 (1986).
[7] H. G. Winful, Opt. Lett. **11**, 33 (1986).
[8] E. Caglioti, S. Trillo, and S. Wabnitz, Opt. Lett. **12**, 1044 (1987).
[9] S. Wabnitz, Phys. Rev. A **38**, 2018 (1988).
[10] G. Cappellini and S. Trillo, Phys. Rev. A **44**, 7509 (1991).
[11] S. Trillo and S. Wabnitz, Phys. Lett. A **159**, 252 (1991).
[12] S. Trillo and S. Wabnitz, in *Nonlinearity with Disorder*, edited by F. Abdullaev, A. R. Bishop, and S. Pnevmatikos (Springer, Berlin, 1992), p. 269.
[13] S. G. Murdoch, R. Leonhardt, and J. D. Harvey, Opt. Lett. **20**, 866 (1995).
[14] P. Drummond, T. A. B. Kennedy, J. M. Dudley, R. Leonhardt, and J. D. Harvey, Opt. Commun. **78**, 137 (1990).
[15] J. E. Rothenberg, Phys. Rev. A **42**, 682 (1990).
[16] S. Trillo and S. Wabnitz, J. Opt. Soc. Am. B **6**, 238 (1989); **9**, 1061 (1992).
[17] E. A. Golovchenko and A. N. Pilipetskii, Sov. Lightwave Commun. **1**, 271 (1991).
[18] C. De Angelis, M. Santagiustina, and S. Trillo, Phys. Rev. A **51**, 774 (1995).
[19] S. Trillo, S. Wabnitz, R. H. Stolen, G. Assanto, C. T. Seaton, and G. I. Stegeman, Appl. Phys. Lett. **49**, 1224 (1986).
[20] S. F. Feldman, D. A. Weinberger, and H. G. Winful, Opt. Lett. **15**, 311 (1990).
[21] E. A. Coddington and N. Levison, *Theory of Ordinary Differential Equations* (McGraw-Hill, New York, 1955), pp. 78–81.
[22] W. Zhao and E. Bourkoff, IEEE J. Quantum Electron. **29**, 2198 (1993).